THE ASTROPHYSICAL JOURNAL, 355:651–660, 1990 June 1

THE FORMATION PHASE OF THE SOLAR NEBULA[1]

PETER BODENHEIMER
University of California Observatories/Lick Observatory, Board of Studies in Astronomy and Astrophysics, University of California, Santa Cruz; and Max-Planck-Institut für Physik und Astrophysik, Garching, FRG

HAROLD W. YORKE
Institut für Astronomie und Astrophysik, Universität Würzburg, FRG

MICHAŁ RÓŻYCZKA
Warsaw University Observatory

AND

JOEL E. TOHLINE
Department of Physics and Astronomy, Louisiana State University
Received 1989 September 1; accepted 1989 December 4

ABSTRACT

Hydrodynamical calculations of the collapse of an axisymmetric, rotating protostellar cloud, with radiation transport and without magnetic fields, are presented. The collapse is assumed to start from a centrally condensed sphere of radius 5×10^{15} cm, a mean density of 4×10^{-15} g cm^{-3}, a total mass of 1 $M_\odot$ and a total angular momentum of 10^{53} g cm^2 s^{-1}. The numerical grid is chosen to resolve the region of disk formation between 1 and 60 AU from the center. The calculations are continued until a relatively thick, warm disk, close to hydrostatic equilibrium, is formed. Frequency-dependent radiative transfer calculations show how the emergent spectrum of the structure depends upon viewing angle with respect to the rotation axis and how the observed isophotal contours should depend on wavelength and viewing angle. The central part of the protostar, interior to 1 AU, is not resolved numerically but is modeled approximately. At the end of the calculation this region is found to have a mass of 0.6 $M_\odot$ and a ratio of rotational to gravitational energy of ~ 0.4, sufficiently large to be unstable to nonaxisymmetric perturbations. Although the disk is gravitationally stable according to the local Toomre criterion, the nonaxisymmetric structure in the center is likely to lead to angular momentum transport.

Subject headings: hydrodynamics — solar system: general — stars: formation — stars: circumstellar shells

I. THE PHYSICAL PROBLEM

Recent models of the evolution of the solar nebula are constructed under the assumptions that the disk is thin and has negligible self-gravity; the calculations start from arbitrary initial conditions (Ruden and Lin 1986; Ruzmaikina and Maeva 1986; Cabot *et al.* 1987*a*, *b*). However, the likely distributions of mass and angular momentum in collapsing interstellar clouds indicate that at least in the early phases the nebula is likely to be relatively massive in comparison with the central protostellar core. The structure of this initial nebula is important in that it determines the processes and timescale for redistribution of angular momentum in the early phases of evolution. Therefore, the main question to be investigated in this paper is: *What is the likely structure of the solar nebula immediately after the collapse of its parent interstellar cloud?* A related question of importance is: *What is the predicted appearance of the emergent spectrum and isophotal contours of the system during the formation phase?* The formation phase is here defined as that phase during which the system is composed of a central stellar-like core in hydrostatic equilibrium, a surrounding circumstellar disk, and an outer, optically thick infalling rotating envelope. Two-dimensional hydrodynamic calculations of the collapse of a rotating protostar, in connection with frequency-dependent radiative transport, are presented here in an analysis of these questions.

The choice of initial conditions for the collapse is subject to some uncertainty. However, it is generally accepted that stars of low mass (~ 1 $M_\odot$) form from the collapse of the dense cores of molecular clouds, which have typical densities of 10^5 particles cm^{-3} and temperatures of 10–20 K (Shu, Adams, and Lizano 1987). These cores are somewhat centrally condensed, but they have no observed collapse motions, so it is not certain what the density distribution at the start of collapse is. This distribution is determined in part by the process of decoupling of the magnetic field from the gas (Mestel and Spitzer 1956). Magnetic support of cloud material against the force of gravity is likely at densities lower than that of the cloud cores (Shu, Adams, and Lizano 1987; Heyer 1988). Models of turbulent, magnetic cloud cores with ambipolar diffusion presented by Shu *et al.* (1988) indicate that rapid evolution, leading to collapse, starts when the density at the center increases to 10^5–10^6 cm^{-3}. At this point the magnetic field has not yet decoupled from the gas; however, magnetic forces are no longer strong enough to prevent collapse. Estimates of the critical density above which decoupling occurs range from 10^9–10^{11} cm^{-3} (Nakano 1984, 1985) to 10^4–10^6 cm^{-3} (Mouschovias, Paleologou, and Fiedler 1985); however these densities are not necessarily those at which collapse starts. In the present calculations, mean starting densities of $\approx 10^9$ cm^{-3} are employed; such values are probably somewhat higher than actual values at the very beginning of collapse, but they are to some extent determined by computational requirements (§ II).

A closely related question is that of choosing the appropriate

[1] UCO/Lick Observatory Bulletin, No. 1157.

initial conditions so that the likely outcome is a single star rather than a binary. A recent survey by Halbwachs (1986) indicates that the fraction of single stars is at most 23%, while Abt (1983) finds that at least 84%, and probably closer to 100%, of solar-type stars with normal abundances are multiple. Several hypotheses have been put forward to explain under what circumstances a single star is formed. An initial specific angular momentum in the range $j \approx 10^{19}$ cm^2 s^{-1} could be sufficiently low to prevent binary formation (Boss 1985; Safronov and Ruzmaikina 1985). However, the orbits of the outer planets have $j \approx 10^{20}$ cm^2 s^{-1}, so that outward transport of mass and angular momentum on a reasonable time scale would be required. A second possibility involves a higher specific angular momentum of $j \approx 10^{20}$ cm^2 s^{-1}. According to Boss (1987), an initially uniform density is likely to lead to fragmentation into a binary, while a centrally condensed distribution leads to a single star. The difficulty here is that if star formation is initiated in the dense cores of molecular clouds by a gradual process of diffusion of the gas relative to the magnetic field (Shu, Adams, and Lizano 1987), the initial distribution of gas when collapse starts must be centrally condensed, approximating a singular isothermal sphere with density $\rho \propto R^{-2}$, where R is the distance to the center. Therefore, most low-mass stars should be single, contrary to observation. As a third possibility, Pringle (1989) has suggested, in view of the above problem, that single stars form by the process outlined by Shu, Adams, and Lizano (1987) but that binary star formation is induced by collisions between cloud cores. As a further (fourth) scenario, Miyama (1989) proposes that single stars are formed from cloud cores with $j \approx 10^{21}$ cm^2 s^{-1}, with thermal, rotational, and gravitational energies in the range where they are stable to fragmentation according to numerical simulations (Miyama, Hayashi, and Narita 1984). Such a cloud would be expected to first reach a rotationally supported equilibrium that is stable to fragmentation but unstable to nonaxisymmetric perturbations. The instabilities would lead to angular momentum transport (Durisen *et al.* 1986), resulting in the collapse of a central condensation. A final suggestion for the formation of a single star involves its formation by the spiraling together of binary condensations (Boss 1987). These suggestions, evaluated together, lead us to assume that a reasonable initial condition for the formation of the solar nebula is a centrally condensed isothermal cloud, at rest, with j at the outer edge $\approx 3 \times 10^{20}$ cm^2 s^{-1}. A value of j in this range is consistent with the orbital angular momentum of the giant planets, it falls within the observed range deduced for cloud cores (Goldsmith and Arquilla 1985; Heyer 1988), and it is in many cases found to provide reasonable agreement between the spectra of model protostars and observed embedded infrared sources (Adams, Lada, and Shu 1987).

A further problem associated with the formation of the solar nebula concerns the redistribution of angular momentum. Most of the low-mass T Tauri stars have rotational velocities of 20 km s^{-1} or less (Hartmann *et al.* 1986; Hartmann, Soderblom, and Stauffer 1987). The distribution of angular momentum in a molecular cloud core with any reasonable density distribution does not agree with that of a T Tauri star plus disk, with the same total mass and angular momentum (Cassen, Shu, and Terebey 1985; Bodenheimer *et al.* 1988). The required outward transport of angular momentum is unlikely during the collapse itself. Magnetic torques (Hoyle 1960; Hayashi 1981; Mouschovias 1987) will be negligible because the initial densities chosen here are high enough so that the field is decoupled from the matter. The very inner regions near the protosun may eventually become partially ionized, but those regions are not resolved in these calculations, and, in any case, magnetic transport will not be effective beyond 1 AU (Hayashi 1981; Safronov and Ruzmaikina 1985). Turbulent viscosity will not be important during the collapse, first, because there is no identifiable mechanism to cause turbulence before disk formation, and second because the turbulence, if any, will be subsonic, and soon after the collapse starts the free fall time will be much shorter than the sound crossing time (Morfill, Tscharnuter, and Völk 1985). We also assume that initial nonaxisymmetric perturbations are small. Such perturbations tend to be amplified during collapse (Boss 1989), but the time scales are such that the main effect of the resulting angular momentum transport will take place after the collapse, once the disk has settled into equilibrium. For all these reasons it is reasonable to assume that the collapse can be calculated with conservation of angular momentum of each mass element. However, one or more of the processes just mentioned must operate during the subsequent evolution of the disk, so that the angular momentum redistribution problem can be solved.

Modern theoretical work on the problem of formation of the solar nebula goes back to the work of Cameron (1962, 1963) who discussed in a semiquantitative way the collapse of a cloud to form a disk. Analytical and numerical calculations of the special case of the pressureless rotating cloud collapsing to an equilibrium thin disk have been discussed by Mestel (1963) and by Stemwedel, Yuan, and Cassen (1989). Calculations of the evolution of a thin disk, taking into account the addition of matter from the infalling cloud, have been performed by Cameron (1978), Lin and Bodenheimer (1982), Cassen and Moosman (1981), Cassen and Summers (1983), Cameron (1985), and Ruzmaikina and Maeva (1986). Equilibrium models, in two space dimensions, of the star-disk system have been calculated by Durisen *et al.* (1989) at various times during the accretion process. Semianalytic calculations (Adams and Shu 1986; Adams, Lada, and Shu 1987) of the spectra of protostellar models consisting of a central star, a thin disk, and an optically thick infalling envelope have been compared with a number of observed protostars.

Full two-dimensional hydrodynamical calculations with turbulent viscosity have been reported by Regev and Shaviv (1981) in the isothermal approximation and by Tscharnuter (1981; see also Morfill, Tscharnuter, and Völk 1985 and Tscharnuter 1987*a*) with radiative transfer. Tscharnuter's calculation of a cloud of 3 $M_\odot$, $j = 10^{20}$ cm^2 s^{-1}, starting from a density of 10^{-20} g cm^{-3}, showed the formation of a rapidly rotating equilibrium core of 0.5 $M_\odot$, and gave temperatures in the planet-forming region ranging from 500 K at Mercury's orbit to 15 K at Pluto's. The core would have been unstable to nonaxisymmetric perturbations, leading to angular momentum transport (Yuan and Cassen 1985; Durisen *et al.* 1986). Three-dimensional hydrodynamical calculations of the formation phase for 1 $M_\odot$ have been reported by Boss (1985, 1989), with starting densities of 10^{-18} and 2×10^{-12} g cm^{-3}, respectively. In both cases small initial perturbations grew during collapse and developed nonaxisymmetric structure. Instantaneous time scales for angular momentum transport by gravitational torques were estimated to fall in the range 10^3–10^6 yr.

In this paper we present and discuss the hydrodynamics as well as the spectral and isophotal appearance of two-dimensional models of protostellar formation. The region interior to 1 AU is not calculated explicitly; therefore the complications of the region of dissociation of molecular hydrogen are mostly avoided. The oscillations which are generated there in a one-dimensional calculation (Tscharnuter 1987*b*) are to a considerable extent suppressed in two- or three-dimensional calculations because of the effect of rotation (Tscharnuter 1987*a*), or, even in a spherical calculation, if the initial density is relatively high (Tscharnuter 1987*b*). The main purpose is to improve existing calculations of the disk-forming region in the distance range of 1–60 AU from the center. The computational procedures are discussed in § II, the results in § III, and the conclusions in § IV.

II. THE COMPUTATIONAL PROBLEM

The main problem in calculating the complete collapse of the core of a molecular cloud to its final configuration of a star plus disk is one of length scale. The radius of the final star is $\sim 10^{11}$ cm, while the typical size of the region observed in ammonia in a cloud core is $\sim 10^{17}$ cm. This problem can be handled in one space dimension by adaptive grid techniques (Winkler and Newman 1980) or by joining together solutions applicable in particular regions of the protostar (Stahler, Shu, and Taam 1980). In two or three dimensions the problem becomes quite difficult. In an explicit code, the time step is restricted by the Courant-Friedrichs Lewy (CFL) condition. Therefore, even if the central star is not resolved and the smallest grid cell has size 0.1 AU, the time step becomes $\lesssim 5 \times 10^5$ s, 4 million times smaller than the free-fall time of a cloud starting at a density of 10^{-18} g cm^{-3}. Adams and Shu (1986) used approximate analytical techniques in their models of protostars, rather than a full hydrodynamic treatment. Tscharnuter (1987*a*) used an implicit two-dimensional code with a radially moving grid, in order to resolve the inner regions of a protostar down to a scale of 10^{10} cm. However, the time step still became so short that he was unable to follow the collapse beyond the point where 0.07 $M_\odot$ had collected in the central core and the extent of the disk was ~ 1 AU.

In the present calculation several numerical features are employed. First, the initial mean density is chosen to be 4×10^{-15} g cm^{-3}, with a mean free-fall time of 1000 yr. The smallest zone is 1 AU in width, corresponding to a CFL time step of $\lesssim 5 \times 10^6$ s. This choice allows the calculation to be carried out in ~ 8 hr of Cray time (25,000 time steps). It is of course important to determine whether the above density is the correct one, at which the magnetic field becomes unimportant.

Second, the central region of the protostar, with approximate radius of 1 AU, is not resolved. Mass is allowed to flow into that region, but not out of it. At every time step, the core mass M_c, the core angular momentum J_c, and the rate of mass flow across the boundary $\dot{M}$ are calculated. The core is assumed to be approximated by a Maclaurin spheroid, in hydrostatic equilibrium. For a given (M_c, J_c, T_c) where T_c is the mean temperature of the core material, the equilibrium structure of the spheroid can be determined through an iterative procedure as described by Tohline (1981, 1984). For a given mean core density, we have adopted a temperature that places the core on the (ρ, T) path traced out by the *center* of the protostar modeled by Winkler and Newman (1980). From the determined equilibrium structure, quantities such as the equatorial radius R_e and the ratio β of the rotational energy to the absolute value of the gravitational energy can be calculated. Under the assumption that most of the mass accreted by the central object arrives near the equatorial plane and that all of the infall kinetic energy is converted to radiation in the shock and boundary layer, the accretion luminosity can be calculated according to $L = 0.5GM_c \dot{M}/R_e$. In a time step Δt the energy $L\,\Delta t$ is added to the central zone as thermal energy and is used as an inner boundary condition for the radiative transfer calculations. The central zone provides most of the energy that goes into heating and radiative losses in the envelope.

A third procedure involves the use of two different numerical grids, both with 60 zones each in the cylindrical coordinate directions R and Z. The zones are slightly concentrated toward the axes to improve the resolution there, but the zone sizes $\Delta R_j \approx \Delta R_{j+1}$ for all j and $\Delta R = \Delta Z$ at $R = Z$, to maintain second order accuracy. The outer grid has a size $R_1 = Z_1 = 5 \times 10^{15}$ cm, and its innermost zone has a radius of 5.5×10^{13} cm. The calculation is first done on this grid with fixed outer values of density and temperature. At 10 different times during the calculation all physical quantities at the boundary of an inner cylinder of radius $R_2 = 10^{15}$ cm and half-height $Z_2 = 10^{15}$ cm are stored. These quantities serve as time-dependent boundary conditions for a second calculation on the inner grid, whose resolution is ~ 5 times finer and whose innermost zone has a radius of 1.5×10^{13} cm.

The equations that are solved are the standard equations of hydrodynamics with radiation transport, and the Poisson equation for the gravitational potential (Black and Bodenheimer 1975, their eqs. [1]–[4]). The two-dimensional hydrodynamic code of Różyczka (1985) is employed. The Poisson equation is solved according to the diffusion technique described by Black and Bodenheimer (1975). Physical viscosity is not included, and angular momentum transport during the collapse is assumed to be negligible. The equation of state is that of an ideal gas, including molecular dissociation.

The numerical method for radiation transfer is not exact because it does not involve a solution for the frequency-dependent radiation intensity and the two-dimensional temperature distribution simultaneously, a procedure that is possible in practice only in the one-dimensional case. Instead, the solution of a flux-limited, frequency-independent, diffusion equation is included along with the hydrodynamics, and the frequency-dependent spectral and isophotal appearance of the models is calculated as a separate step, after the hydrodynamic calculation has been completed. The region between 1.5×10^{13} cm and 5×10^{15} cm is initially optically thick, so the diffusion approximation is valid. However, the outer regions become optically thin at later stages of the evolution; a flux limiter is applied so that the solution will be valid in that limit.

The method of solution of the hydrodynamic equations utilizes the principle of operator splitting. The contribution to the time rate of change of the internal energy density e due to the effects of radiation transport is applied in a separate radiation transfer substep. In the limit $|\boldsymbol{u}| \ll c$ we may express this contribution as:

$$\left(\frac{\partial e}{\partial t}\right)_{\rm rad} = \nabla \cdot \boldsymbol{F}\,, \tag{1}$$

where $\boldsymbol{F}$ is the radiative flux, which is calculated according to (Levermore and Pomraning 1981)

$$\boldsymbol{F} = -\frac{c\lambda}{\rho\kappa}\,\nabla e_r\,. \tag{2}$$

Here, λ is called the flux-limiter, κ is the opacity (see below), and e_r is the radiation energy density. In the following we shall assume radiative equilibrium, so that $e_r = aT^4$, where a is the radiation density constant.

By a proper choice of the flux-limiter λ it is possible to obtain a solution sufficiently accurate for our present needs. We first note that in the optically thick limit $\rho\kappa\,\Delta l \to \infty$ (Δl is a typical length scale for the problem), we expect $\lambda \to \frac{1}{3}$, i.e., the *diffusion* limit. In the optically thin limit $\rho\kappa\,\Delta l \to 0$ we expect the *streaming* limit, i.e., $|\boldsymbol{F}| \to ce_r$. This is simply a restatement of causality: the ratio of radiative flux to radiative energy density cannot exceed the speed of light. Because we can expect scattering to be negligible in the mid-IR and far-IR regimes of interest, we write the dimensionless parameter R used by Levermore and Pomraning (1981) in the form:

$$R = \frac{|\nabla e_r|}{e_r \rho\kappa} \tag{3}$$

and use their simple rational approximation for the flux-limiter:

$$\lambda(R) = \frac{2 + R}{6 + 3R + R^2} . \tag{4}$$

Note that in the above discussion we employ frequency-averaged quantities to represent the opacity and the radiative flux. For the flux-limited diffusion equations, we use the frequency-averaged opacities of Pollack, McKay, and Christofferson (1985), who have updated estimates of the Rosseland mean opacity of dust grains in regimes of interest for protostellar collapse. These opacities are supplemented by those of Alexander (1975) for the regions where molecules dominate.

For the numerical solution of the above set of equations we approximate the factor $\lambda/\rho\kappa$ in equation (2) by its value at the previous time step, keeping it constant for the duration of the time step. Combining equations (1) and (2) thus yields a partial differential equation, the structure of which is parabolic. For stability reasons the time derivative $(\partial e/\partial t)_{\rm rad}$ should be discretized using backward differences. Forward time differencing would lead to prohibitively small time steps. The spatial differencing can be done in a straightforward space-centered manner. The resulting difference equations must be solved iteratively. We have developed an ADI procedure, similar to the recipe given by Marsal (1976; see p. 144ff). Typically, we require 10–20 iterations for convergence.

The frequency-dependent spectral and isophotal appearance of the models must be calculated as a separate step following computation of the hydrodynamical models (as in Bertout and Yorke 1978; Yorke 1986; see also Bodenheimer *et al.* 1988). We use an axially symmetric version of the three-dimensional ray-tracing procedure outlined by Yorke (1986, his eqs. 2.1, 2.2, and 2.3abc). The equation for transfer of radiation intensity is solved numerically on a grid of lines of sight through the protostellar envelope for a grid of frequencies and at given "viewing" angles. At each point along the line of sight the frequency-dependent source function and opacities are calculated as a function of the density and local grain temperature. The ray-tracing solution is obtained for 18 frequencies logarithmically equidistant in the interval between 1.6 cm^{-1} and 4×10^3 cm^{-1}. The emerging flux from each line of sight grid point, at each frequency and for each viewing angle considered, is stored for later use. The overall spectrum for a given viewing angle, for instance, is obtained by a straightforward spatial integration over all lines of sight. By spatial integration over a subset of lines of sight we obtain the spectrum at a particular offset; the assumed beam size can be varied. Isophotal maps give the full spatial information for a particular frequency. This procedure has been applied to three-dimensional models of the early stages of protostellar evolution by Boss and Yorke (1990).

The principal source of opacity in the protostellar envelope is the dust, which is assumed to arise from refractories (i.e., graphites and silicates) that exist at temperatures $T_R \lesssim 1700$ K, as well as from volatiles (i.e., water, ammonia, and methane ices) which only exist at temperatures $T_V \lesssim 150$ K. The frequency-dependent opacities have been computed by Yorke (1979). Rosseland means of these opacities (see Fig. 2-1 of Yorke 1988) are consistent with the opacities of Pollack, McKay, and Christofferson (1985), which were used for the hydrodynamic calculations. For grain temperatures in excess of 150 K the opacities are also consistent with those of Draine and Lee (1984), who did not consider a volatile component.

A more accurate radiation transfer calculation could in principle be made by updating the grain temperatures—say, under the assumption of radiative equilibrium for each component of dust—after the radiation intensity at each point along the line of sight for all frequencies and viewing angles has been calculated. An exact radiation transfer calculation could then be made by iterating between ray tracing and such temperature updates, until the temperature distribution has converged. However, although efficient numerical methods exist in one-dimension for calculating the radiation intensity exactly and even simultaneously with the hydrodynamics, they cannot be easily generalized to two or three dimensions (Yorke 1986). A prohibitive amount of CPU time would be necessary with present-day computers. Exact two- and three-dimensional frequency-independent calculations of poor spatial and angular resolution are now just barely feasible (see, e.g. Knölker and Schüssler 1988; Nordlund 1986 and references therewithin). Considering the numerical effort and the fact that the initial conditions and boundary conditions for the hydrodynamical calculations are poorly known, we have not attempted to update the temperature distribution obtained from the hydrodynamic calculations. Our spectra and isophotal appearances are therefore more of a qualitative nature than rigorously exact. For early evolutionary phases with relatively high optical depths, the temperature distributions obtained from the flux-limited diffusion approximation can be considered reasonably accurate. This statement, of course, can only be justified rigorously in one-dimensional test calculations. Such calculations have been performed by Kley (1989) in a somewhat different context (accretion onto a white dwarf) and by Yorke (1986), using a different flux-limiter than that employed here. Nearly exact temperature distributions can be obtained by "fine tuning" flux limiter parameters for the problem at hand. However, it is not clear whether a "tuned" flux limiter then performs equally well for the two-dimensional problem as it has in one dimension. Yorke (1986) finds that his untuned flux limiter tends to underestimate the temperatures in dusty protostellar envelopes, typically by 10%–15%, so that the near infrared fluxes would also be underestimated.

III. RESULTS

The calculation starts with a mass of 1 $M_\odot$ at rest in a sphere of radius 5×10^{15} cm. The density distribution is taken to be $\rho \propto r^{-2}$, where r is the distance to the origin. The temperature T is taken to be uniform at 20 K. At this T the sphere is not in equilibrium in the absence of the field; the ratio α of

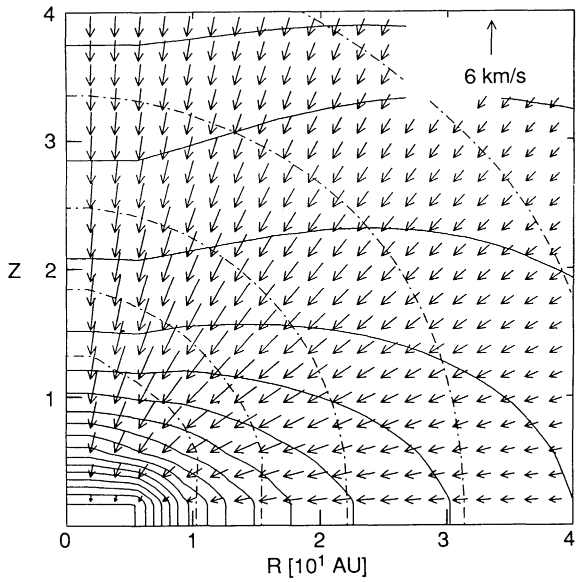

FIG. 1.—The structure of the inner part of the cloud shortly after the beginning of collapse (763 yr). The Z-axis corresponds to the rotation axis and the R-axis to the equatorial plane. *Solid curves*: equidensity contours for densities (in c.g.s.) ranging from $\log \rho = -10.4$ (*center*) to -13.6 (*outer edge*), with contour interval $\Delta \log \rho = 0.2$. *Dash-dotted curves*: isotherms for temperatures ranging from $\log T = 3.0$ (*center*) to 2.6 (*outer edge*), with contour interval $\Delta \log T = 0.1$. *Arrows*: velocity vectors with length proportional to speed. The velocity scale is given at the upper right.

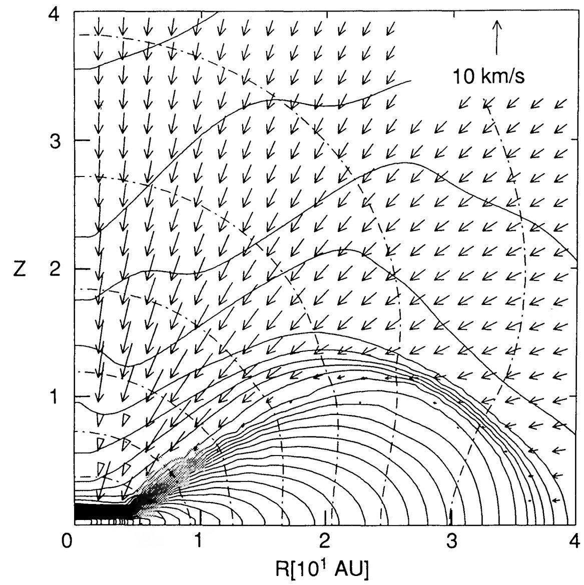

FIG. 2.—Structure of the inner part of the cloud after 2026 yr. Symbols have the same meaning as in Fig. 1, and the contour intervals are the same. Densities range from $\log \rho = -8.6$ to -15.4 and temperature from $\log T = 2.9$ to 2.3. Open triangles indicate velocities greater than 10 km s^{-1}.

thermal energy to the absolute value of the gravitational energy is 0.08. The initial angular velocity is $\Omega = 10^{-11}$ s^{-1}, giving a total angular momentum of 10^{53} g cm^2 s^{-1} and a mean specific angular momentum (j) of 5×10^{19} cm^2 s^{-1}. The value of j for the outermost equatorial mass element is 2.5×10^{20} cm^2 s^{-1}, corresponding to an equilibrium radius for centrifugal balance of 30 AU. The ratio β of initial rotational energy to the absolute value of the gravitational energy is 0.01.

Calculations were followed on the outer grid for 2790 yr. The temperature immediately starts to increase, reaching a maximum of ~ 1500 K just outside the core (7×10^{13} cm). The density contours are noticeably flattened by rotation; the temperature contours are more nearly spherical. At the end of the calculation infall velocities near the center along the pole are close to free-fall (10 km s^{-1}), and 99.9% of the mass lies within the inner grid of radius 10^{15} cm.

The calculation on the inner grid was started 763 yr after that on the outer grid. The structure of this model is shown in Figure 1. The spatial resolution on the plot is that of the outer grid, ~ 5 AU in the inner regions. The whole structure is in collapse. By 1085 yr after the beginning of collapse (322 yr after the beginning of the calculation on the fine grid), infall at an average velocity of 5 km s^{-1} continues throughout most of the grid, except in a near-equilibrium region of radius 20 AU and height 10 AU which has formed in the center. At this time the central temperature has reached 1318 K, having declined from the maximum of 2200 K that occurred early in the evolution. The midplane temperature is roughly constant with distance out to 9 AU; then it drops approximately as R^{-1}. The mass inflow rate is very rapid at first, with half a solar mass accumulating in the core in the first 10 yr, corresponding to a mean core accretion luminosity of 1.7×10^4 $L_\odot$. During the remainder of the evolution, up to 2500 yr, an additional 0.1 $M_\odot$ reaches the core, corresponding to a mean $\dot{M} = 4 \times 10^{-5}$ $M_\odot$ yr^{-1} and a mean accretion luminosity of ~ 25 $L_\odot$. The remaining mass is added to the "disk" and generates relatively little additional accretion luminosity. An arbitrary minimum luminosity of 200 $L_\odot$ is assigned to the core in this particular calculation, consistent with the high initial density and the fact that the stellar core will lie high on its Hayashi track.

Figure 2, at 2026 yr, shows the well-developed equilibrium structure, 35 AU in radial extent, with an accretion shock on the edge. Its height varies approximately linearly with distance from the central object, out to 20 AU. The region interior to 5 AU is not well resolved by the numerical technique; beyond that point the resolution is good. Note that at $R = 20$ AU, the shock is located four scale heights above midplane. The scale height itself, as a function of radius, is in reasonable agreement with that deduced from the thin disk approximation: $H \approx c_s/\Omega$, where c_s is the sound speed and Ω is the angular velocity. The temperature near the center is now down to 1250 K, reflecting a gradually decreasing accretion rate onto the core, which by now has collected most of the material with low enough angular momentum to reach it. The core mass at this time is 0.58 $M_\odot$, its total angular momentum is 1.5×10^{52} g cm^2 s^{-1}, and its $\beta = 0.44$, indicating instability to nonaxisymmetric perturbations. Figure 3 shows contours of equal rotational velocity at the same time. This pattern remains similar throughout the remaining evolution. In the equilibrium region this velocity is nearly constant on cylinders, as is the temperature (Fig. 2). In an isothermal self-gravitating rotating equilibrium configuration one would expect the angular velocity to be constant on cylinders (Tassoul 1978). Although the structure illustrated is not precisely isothermal, the deviation is not large. A second important feature is the shear layer above the midplane of the disk, where the angular momentum of material arriving on the disk surface is less than that already present in the disk at the same radius (Cassen and Moosman 1981; Ruzmaikina and Maeva 1986). The effect of turbulence generated in this layer will be the subject of further numerical work.

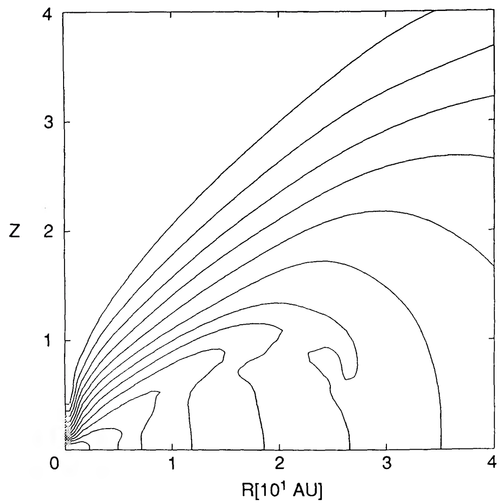

FIG. 3.—Contours of equal rotational velocity v_ϕ for the model shown in Fig. 2. The contour interval is $\Delta \log v_\phi = 0.1$, and the levels range from 5.1 (*upper*) to 6.2 (*center*), in units of cm s^{-1}.

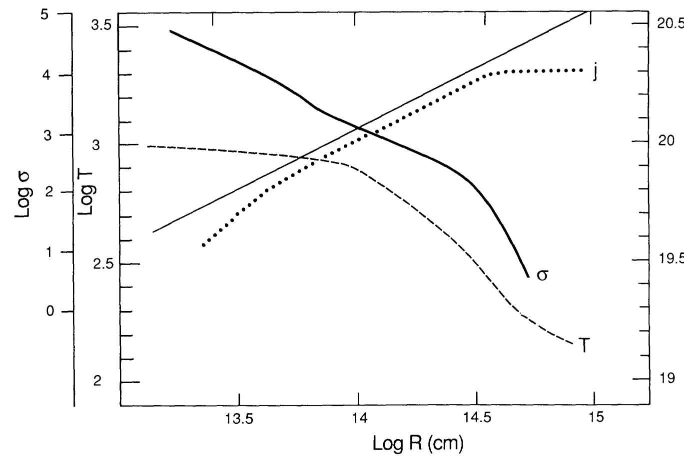

FIG. 5.—Surface density (*solid curve*), midplane temperature (*dashed curve*), and specific angular momentum in the midplane (*dotted curve*) as a function of (cylindrical) radius for the model shown in Fig. 2. The specific angular momentum for Keplerian rotation, for a central mass of 1 $M_\odot$, is shown by the light solid curve.

Figure 4 shows the structure of the model at the last calculated time, 2587 yr. The features are similar to those at the earlier times. Between 30 and 50 AU in the equatorial region the structure is not yet in hydrostatic equilibrium; the expected equilibrium radius is ~ 30 AU. A cooling trend is evident in the midplane temperatures; at this time the inner regions have cooled to 800 K because of the decrease in accretion luminosity onto the central object and the effects of radiative transfer. In fact, heating mechanisms such as turbulence would start to become important at this stage. The core mass at the end of the calculation is 0.61 $M_\odot$, and its angular momentum is 1.54×10^{52} g cm^2 s^{-1}, corresponding to an estimated $\beta = 0.44$.

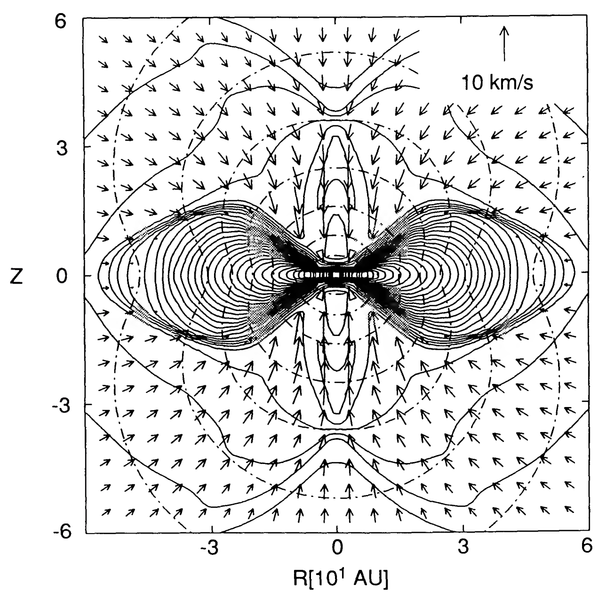

FIG. 4.—Structure of the inner part of the cloud after 2587 yr. Symbols have the same meaning as in Fig. 1, and the contour intervals are the same. Densities range from $\log \rho = -9.8$ to -16, and temperatures from $\log T = 2.9$ to 2.2.

Figure 5 shows the total surface density, the midplane temperature, and the midplane specific angular momentum as a function of radius for the model displayed in Figure 2. By this time most of the mass has joined the disk, so that further changes are small. In the equilibrium region $\sigma \propto R^{-2}$, ranging from 10^4 g cm^{-2} at 2.5 AU to 10^3 g cm^{-2} at 7 AU. The temperature distribution, except for a relatively flat region near the center, varies as R^{-1} in the midplane out to the edge of the equilibrium structure at 30 AU. The angular momentum distribution, in the region 5–30 AU, falls slightly below the Keplerian curve for a central object of 1 $M_\odot$. The mass interior to 5 AU is less than 1 $M_\odot$; therefore the j distribution there deviates somewhat from that Keplerian curve. In the outer regions beyond 30 AU, material is still infalling and has not yet reached its equilibrium radius. These distributions will be modified by angular momentum transport during subsequent nebular evolution, with the result that a large fraction of the mass will land on the central object.

Emergent infrared continuous spectra, as viewed from the equator and the pole, are compared in Figures 6 and 7. During most of the evolution the difference in the two cases is quite small, because the temperature distribution is nearly spherical. Adams and Shu (1986) and Adams, Lada, and Shu (1987) solve the transfer equation by using an equivalent spherical temperature distribution for calculation of the emission, but they include two-dimensional effects in the calculation of the absorption. Qualitatively, our results are consistent with theirs, although a detailed comparison is not possible because their models include both inner regions and outer regions that are not resolved in our calculations. For example, the peak in the spectral energy distribution lies typically in the range 25–60 μm in our models and between 30–50 μm in theirs. Figures 6 and 7 refer to a model at 1416 yr, somewhat earlier than that shown in Figure 2. The wavelength at maximum intensity in the total spectrum makes a slight shift from 40 μm at the pole to 63 μm in the equatorial plane. The spectrum is still dominated by emission from cool dust in the outer regions. At later times (not shown), when the optical depth along the rotation axis becomes very small, the flux from the warm central regions contributes to a larger wavelength shift.

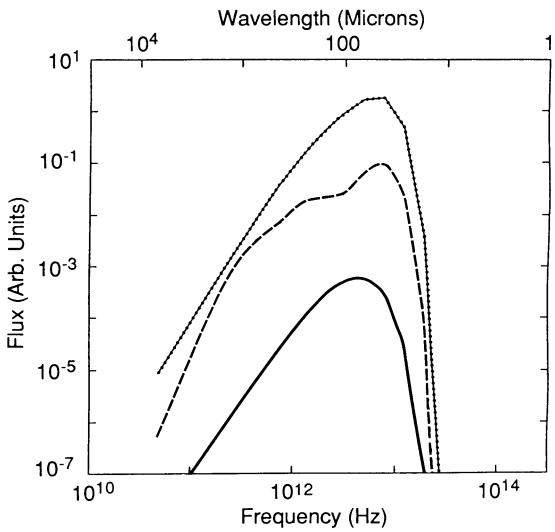

FIG. 6.—The infrared spectrum of a model at 1426 yr, viewed toward the pole. *Filled circles*: the total spectrum, integrated over the entire grid. *Dashed curve*: the spectrum obtained with a very thin beam directed toward the pole. *Solid curve*: the spectrum obtained with a very thin beam offset by 160 AU from the pole and parallel to the rotation axis. The vertical scale is in arbitrary units; the dashed and solid curves are plotted on the same scale, which is different from that used for the total spectrum.

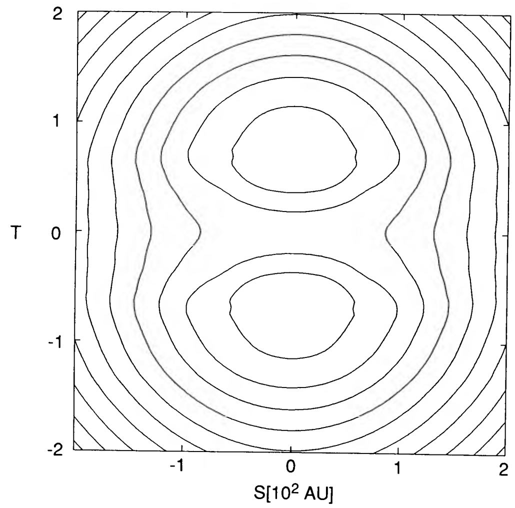

FIG. 8.—Isophotes for a model at 808 yr at a wavelength of 40 μm. The coordinate axes refer to the plane of the sky in a view directed in the equatorial plane. The logarithmically spaced values of the contours are normalized to the maximum value (displaced from the equatorial plane $T = 0$); the contour interval is 0.2 in log intensity.

Figures 8, 9, and 10 show isophotal contours, on the plane of the sky, at a time of 808 yr after the start of collapse. At later times the contours are qualitatively similar, but maxima are compressed more closely to the equatorial plane. Figure 8 shows the contours at 40 μm, viewed in the equatorial plane. Note that the intensity maxima are shifted above and below the plane, because of the high optical depth in it. The effect of a change in inclination angle, at 40 μm, is shown in Figure 9. Here a single maximum starts to dominate, and the contours are noticeably asymmetric. In the limit of the pole-on view the contours are of course circular with a single maximum in the center. The spatial shift in maximum intensity in the equatorial view, which was 80 AU at 40 μm, increases to 125 AU from the plane at 16 μm (Fig. 10) because of the higher dust opacity at that wavelength.

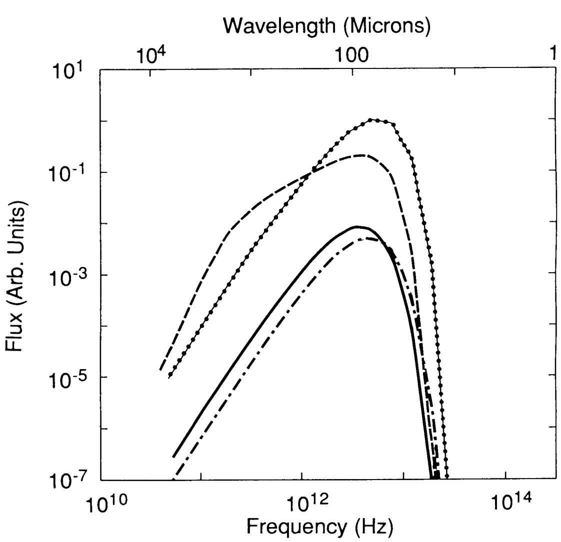

FIG. 7.—The infrared spectrum of the model shown in Fig. 6, as viewed from the equator. *Filled circles*: the total spectrum. *Dashed curve*: the spectrum obtained with a very thin beam directed toward the origin. *Solid curve*: the spectrum obtained with a very thin beam offset by 160 AU from the origin in the plane. *Dot-dashed curve*: the spectrum obtained with a very thin beam offset by 160 AU from the origin along the rotation axis. The last three curves use the same (arbitrary) vertical scale, which differs from that used for the total spectrum.

IV. DISCUSSION AND CONCLUSIONS

The collapse of a rotating interstellar cloud to a final configuration of an equilibrium disk has been followed from a particular set of initial conditions, under the assumption of conservation of angular momentum of individual mass elements. The specific angular momentum at the outer edge in the equatorial plane was taken to be 2.5×10^{20} cm^2 s^{-1}. The

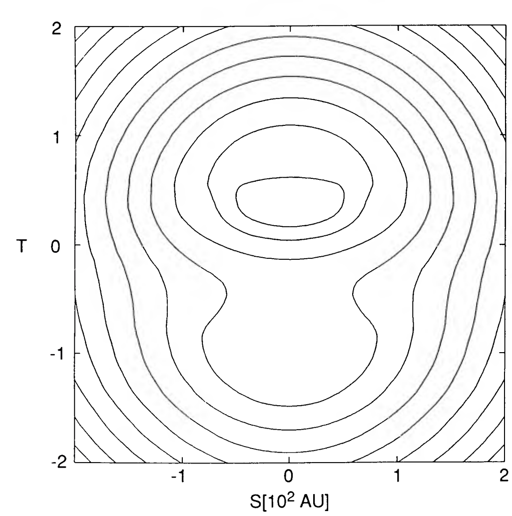

FIG. 9.—Isophotes for the model shown in Fig. 8, at 40 μm, viewed at an inclination angle of 75° with respect to the rotation axis. The contour levels have the same meaning as in Fig. 8.

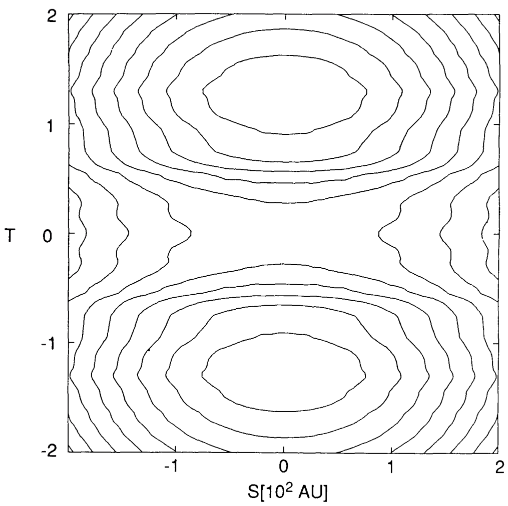

FIG. 10.—Isophotes for the model shown in Fig. 8, at 16 μm, viewed in the equatorial plane. The contour levels have the same meaning as in Fig. 8.

resulting equilibrium structure has a radius of 30 AU and a mass (exterior to 1 AU) $\sim 0.4\ M_\odot$ out of the original $1\ M_\odot$. The possible detection of a disk with similar values of mass and radius around L1551–IRS 5 has been reported by Masson and Keene (1989). The calculated temperature distribution ranges from 1000 K near 1 AU to 150 K near the outer edge, and midplane densities range from 10^{-9} to 10^{-13} g cm^{-3} at 1 AU and 30 AU, respectively. The disk appears relatively thick in the 20–30 AU distance range; however, the density drops rapidly with altitude above the plane, with a scale height ranging from 2.5 AU at 10 AU to 6.5 AU at 30 AU. The accretion shock on the faces of the disk lies 2–4 scale heights above the plane. The thickness of the disk, which is a consequence of the relatively warm temperatures, could be questioned on the numerical grounds that the diffusion approximation underestimates the radiation from behind the shock. However, in this particular case, the temperature in the 20–30 AU region of the disk is determined by the luminosity of the central star which is $\sim 200\ L_\odot$. The radiative flux from the center dominates the flux of kinetic energy of infall of material onto the disk surface. Tests with a reduced central luminosity have been carried out; they show thinner disks whose properties will be outlined in a future paper. The angular velocity does not deviate much from Keplerian rotation.

The region interior to 1 AU is not resolved. It is modeled as a equilibrium structure of mass $0.6\ M_\odot$ and a ratio of rotational to gravitational energy of 0.44. Its estimated equatorial radius is 4×10^{12} cm, much smaller than the size of the first computational zone. Although the model of this core is very approximate, the conclusion that it is unstable to nonaxisymmetric perturbations would be expected to hold even for a more detailed model. Equilibrium rotating polytropic models with a similar angular momentum distribution to that used here indicate dynamical instability to nonaxisymmetric perturbations for β as slow as 0.15 (Durisen *et al.* 1989; S. Yang, R. H. Durisen, and J. Imamura 1989, private communication). Angular momentum transport would therefore be expected to begin rather early in the evolution.

The observable quantities that have been investigated include the total luminosity, the emergent spectrum as a function of viewing angle, and the isophotal contours as a function of viewing angle and frequency. Observationally, of course, extremely high spatial resolution would be required to study the isophotes. The radius of the object in these studies is ~ 300 AU, including the infalling envelope. The mean luminosity, including the accretion luminosity and the intrinsic luminosity of the central object, averages over $250\ L_\odot$, declining gradually toward the end. The typical protostellar candidates investigated by Adams, Lada, and Shu (1987) have luminosities in the range 3.5–53 $L_\odot$, and the luminosities of suspected protostars in the ρ Ophiuchi cluster range from 30 to less than 0.1 $L_\odot$ (Lada 1988). Our computed value is dependent on the assumption of the relatively high initial mean density of 4×10^{-15} g cm^{-3}. A lower value clearly would reduce the computed mean luminosity. Further calculations in this direction are planned.

The overall spectra peak at $\sim 60\ \mu$m in the earlier phases of the evolution. At later phases, as the optical depth in the cool dusty infalling envelope decreases, the peak shifts to $\sim 25\ \mu$m. Protostellar objects can be fitted by theoretical models with peaks in this range (Adams, Lada, and Shu 1987). Comparisons of the detailed spectral energy distributions with those of observed objects will be reserved for future studies. In general, the models show a deficiency in near infrared flux (3 μm) as compared with observed objects, partly because the warm regions with $T > 1000$ K are not resolved in our calculations and partly because our models represent earlier evolutionary times than those of the observed objects. During most of the evolution there is little difference in the overall spectrum as a function of viewing angle. The computations of Adams and Shu (1986) show no change in the energy distribution near the peak of the spectrum as a function of viewing angle. We find there is an effect, but it is relatively small. At the very latest phases, when the infalling envelope has become optically thin in the polar direction, the peak of the spectrum is expected to shift noticeably at the equator with respect to the pole. The calculations reported here stop before this effect is significant.

On the other hand, the isophotal contours show definite differences as a function of viewing angle during the entire evolution. While the contours as viewed from the pole are circles with a central maximum, there is a gradual transition as a function of viewing angle to a structure with two displaced maxima. The separation between the maxima increases with decreasing wavelength and can be as large as, for example, 300 AU in the equatorial plane at 16 μm.

The stability of the structure shown in Figure 4, and its subsequent evolution, are important questions. Of particular interest is the implication regarding the formation times of the giant planets. Lissauer (1987) and Wetherill (1989) have shown that if the surface density of condensible solids falls in the range 15–30 g cm^{-2}, Jupiter's core could form by runaway accretion of solid particles on the relatively short time scale of 5×10^5–10^6 yr. The corresponding total surface density is 1500–3000 g cm^{-2}, and, in fact, the calculated model has $\sigma = 3000$ at 5 AU. The crucial question then is: what is the time scale for significant evolution of the nebula, assuming the solid material evolves with the gas, compared with the accretion time for Jupiter?

Inward mass transport and outward angular momentum transport could result from gravitational instability, from viscous diffusion, or from the gravitational torques generated by the central object. The disk obtained in the present calculations turns out to be gravitational stable to axisymmetric perturbations. The Toomre Q parameter [$\propto \Omega c_s/(G\sigma)$, where the epicyclic frequency is approximated by Ω] has been calculated to be 4, 7, and 10 at radii of 5, 10, and 20 AU, respectively. According to Adams, Ruden, and Shu (1989), a non-axisymmetric gravitational instability is also possible, but their results for thin disks indicate that growth rates are very slow for Q at corotation greater than 3. Nevertheless, the central object will transfer angular momentum to the nebula to an unknown extent. Convective instability in the vertical direction will occur in these models because of the temperature dependence of the grain opacities (Lin and Papaloizou 1980). The evolutionary time scale is uncertain; for a nebular mass of 0.05 $M_\odot$, Ruden and Lin (1986) estimate an evolution time of 4×10^5 yr, similar to the time for runaway accretion of a giant planet. For a more massive nebula, their results indicate that the evolution time would be shorter. However, Cabot *et al.* (1987*a*, *b*) give somewhat longer time scales for convective evolution.

While the infall is still taking place onto the disk surface, turbulence generated in the shear layer could again cause transport, with an uncertain time scale. Propagation of sound waves and dissipation by shocks could also transport angular momentum on time scales similar to that by convection (Larson 1989); however, refraction of the waves and dissipation as they propagate in the vertical direction probably limit the effectiveness of this process (Lin, Papaloizou, and Savonije 1990). An analysis in three space dimensions is required for consideration of the effects of gravitational torques, either from the amplification of initial non-axisymmetric perturbations (Boss 1985, 1989) or from barlike perturbations that could develop in the unstable central core, Many of the above effects have comparable time scales, and the processes of gap clearing and orbital migration of the protoplanet (Lin and Papaloizou 1986) also must be taken into account. Therefore the coupled evolution of forming protoplanets and the solar nebula, taking into account a variety of complicated processes, represents an important problem for future study.

This work was supported in part through National Science Foundation grant AST-8521636 and in part through a special NASA astrophysics theory program which supports a joint Center for Star Formation Studies at NASA/Ames Research Center, University of California, Berkeley, and University of California, Santa Cruz. P. B. thanks the Alexander von Humboldt Foundation for a US Senior Scientist Award, and three of us (P. B., H. W. Y., M. R.) thank the Max-Planck-Institut für Physik und Astrophysik in Garching, West Germany, for their hospitality and support. H. W. Y. acknowledges support from DFG grant Yo 5/3-2. P. B. thanks the San Diego Supercomputer Center for a grant of computer time.

REFERENCES

Abt, H. A. 1983, *Ann. Rev. Astr. Ap.*, **21**, 343.
Adams, F. C., Lada, C. J., and Shu, F. H. 1987, *Ap. J.*, **312**, 788.
Adams, F. C., Ruden, S. P., and Shu, F. H. 1989, *Ap. J.*, **347**, 959.
Adams, F. C., and Shu, F. H. 1986, *Ap. J.*, **308**, 836.
Alexander, D. 1975, *Ap. J. Suppl.*, **29**, 363.
Bertout, C., and Yorke, H. W. 1978, in *Protostars and Planets*, ed. T. Gehrels (Tucson: University of Arizona Press), p. 648.
Black, D. C., and Bodenheimer, P. 1975, *Ap. J.*, **199**, 619.
Bodenheimer, P., Różyczka, M., Yorke, H. W., and Tohline, J. E. 1988, in *Formation and Evolution of Low-Mass Stars*, ed. A. K. Dupree and M. T. V. T. Lago (Dordrecht: Kluwer Academic), p. 139.
Boss, A. P. 1985, *Icarus*, **61**, 3.
———. 1987, *Ap. J.*, **319**, 149.
———. 1989, *Ap. J.*, **346**, 336.
Boss, A. P., and Yorke, H. W. 1990, *Ap. J.*, submitted.
Cabot, W., Canuto, V. M., Hubickyj, O., and Pollack, J. B. 1987*a*, *Icarus*, **69**, 387.
———. 1987*b*, *Icarus*, **69**, 423.
Cameron, A. G. W. 1962, *Icarus*, **1**, 13.
———. 1963, *Icarus*, **1**, 339.
———. 1978, *Moon and Planets*, **18**, 5.
———. 1985, in *Protostars and Planets II*, ed. D. C. Black and M. S. Matthews (Tucson: University of Arizona Press), p. 1073.
Cassen, P., and Moosman, A. 1981, *Icarus*, **48**, 353.
Cassen, P., Shu, F. H., and Terebey, S. 1985, in *Protostars and Planets II*, ed. D. C. Black and M. S. Matthews (Tucson: University of Arizona Press), p. 448.
Cassen, P., and Summers, A. 1983, *Icarus*, **53**, 26.
Draine, B. T., and Lee, H. M. 1984, *Ap. J.*, **285**, 89.
Durisen, R. H., Gingold, R. A., Tohline, J. E., and Boss, A. P. 1986, *Ap. J.*, **305**, 281.
Durisen, R. H., Yang, S., Cassen, P., and Stahler, S. W. 1989, *Ap. J.*, **345**, 959.
Goldsmith, P. F., and Arquilla, R. 1985, in *Protostars and Planets II*, ed. D. C. Black and M. S. Matthews (Tucson: University of Arizona Press), p. 137.
Halbwachs, J. L. 1986, *Astr. Ap.*, **168**, 161.
Hartmann, L., Hewett, R., Stahler, S., and Mathieu, R. D. 1986, *Ap. J.*, **309**, 275.
Hartmann, L., Soderblom, D., and Stauffer, J. 1987, *A.J.*, **93**, 907.
Hayashi, C. 1981, *Progr. Theor. Phys. Suppl.*, **70**, 35.
Heyer, H. M. 1988, *Ap. J.*, **324**, 311.
Hoyle, F. 1960, *Quart. J.R.A.S.*, **1**, 28.
Kley, W. 1989, *Astr. Ap.*, **208**, 98.
Knölker, M., and Schüssler, M. 1988, *Astr. Ap.*, **202**, 275.
Lada, C. 1988, in *Formation and Evolution of Low-Mass Stars*, ed. A. K. Dupree and M. T. V. T. Lago (Dordrecht: Kluwer Academic), p. 93.
Larson, R. B. 1989, in *The Formation and Evolution of Planetary Systems*, ed. H. A. Weaver and L. Danly (Cambridge: Cambridge University Press), p. 31.
Levermore, C. D., and Pomraning, G. C. 1981, *Ap. J.*, **248**, 321.
Lin, D. N. C., and Bodenheimer, P. 1982, *Ap. J.*, **262**, 768.
Lin, D. N. C., and Papaloizou, J. 1980, *M.N.R.A.S.*, **191**, 37.
———. 1986, *Ap. J.*, **309**, 846.
Lin, D. N. C., Papaloizou, J., and Savonije, J. 1990, *Ap. J.*, submitted.
Lissauer, J. J. 1987, *Icarus*, **69**, 249.
Marsal, D. 1976, *Die numerische Lösung partieller Differentialgleichungen* (Mannheim: B. I.-Wissenschaftsverlag).
Masson, C., and Keene, J. 1989, paper presented at the Centennial Meeting of the Astronomical Society of the Pacific, 1989 June 21–23.
Mestel, L. 1963, *M.N.R.A.S.*, **126**, 553.
Mestel, L., and Spitzer, L., Jr. 1956, *M.N.R.A.S.*, **116**, 505.
Miyama, S. 1989, in *The Formation and Evolution of Planetary Systems*, ed. H. A. Weaver and L. Danly (Cambridge: Cambridge University Press), p. 284.
Miyama, S., Hayashi, C., and Narita, S. 1984, *Ap. J.*, **279**, 621.
Morfill, G. E., Tscharnuter, W., and Völk, H. J. 1985, in *Protostars and Planets II*, ed. D. C. Black and M. S. Matthews (Tucson: University of Arizona Press), p. 493.
Mouschovias, T. Ch. 1987, in *Physical Processes in Interstellar Clouds*, ed. G. E. Morfill and M. Scholer (Dordrecht: Reidel), p. 491.
Mouschovias, T. Ch., Paleologou, E. V., and Fiedler, R. A. 1985, *Ap. J.*, **291**, 772.
Nakano, T. 1984, *Fund. Cosmic Phys.*, **9**, 139.
———. 1985, *Pub. Astr. Soc. Japan*, **37**, 69.
Nordlund, A. 1986, in *Small-Scale Magnetic Flux Concentrations in the Solar Photosphere*, ed. W. Deinzer, M. Knölker, and H. H. Voigt (Göttingen: Vanderhoeck and Ruprecht), p. 83.
Pollack, J. B., McKay, C., and Christofferson, B. 1985, *Icarus*, **64**, 471.
Pringle, J. E. 1989, *M.N.R.A.S.*, **239**, 361.
Regev, O., and Shaviv, G. 1981, *Ap. J.*, **245**, 934.
Różyczka, M. 1985, *Astr. Ap.*, **143**, 59.
Ruden, S. P., and Lin, D. N. C. 1986, *Ap. J.*, **308**, 883.
Ruzmaikina, T. V., and Maeva, S. V. 1986, *Astr. Vestn.*, **20**, 212.
Safronov, V. S., and Ruzmaikina, T. V. 1985, in *Protostars and Planets II*, ed. D. C. Black and M. S. Matthews (Tucson: University of Arizona Press), p. 959.
Shu, F. H., Adams, F. C., and Lizano, S. 1987, *Ann. Rev. Astr. Ap.*, **25**, 23.
Shu, F., Lizano, S., Adams, F. C., and Ruden, S. P. 1988, in *Formation and Evolution of Low-Mass Stars*, ed. A. K. Dupree and M. T. V. T. Lago (Dordrecht: Kluwer Academic), p. 123.
Stahler, S. W., Shu, F. H., and Taam, R. E. 1980, *Ap. J.*, **241**, 637.
Stemwedel, S. W., Yuan, C., and Cassen, P. 1989, preprint.
Tassoul, J.-L. 1978, *Theory of Rotating Stars* (Princeton: Princeton University Press).
Tohline, J. E. 1981, *Ap. J.*, **248**, 717.
———. 1984, *Ap. J.*, **285**, 721.
Tscharnuter, W. 1981, in *Fundamental Problems in the Theory of Stellar Evolution*, ed. D. Sugimoto, D. Q. Lamb, and D. N. Schramm (Dordrecht: Reidel), p. 105.
———. 1987*a*, *Astr. Ap.*, **188**, 55.

Tscharnuter, W. 1987*b*, *Lecture Notes in Physics*, in *Physical Processes in Comets, Stars, and Active Galaxies*, ed. E. Meyer-Hofmeister, H. C. Thomas, and W. Hillebrandt (Berlin: Springer-Verlag).
Wetherill, G. W. 1989, in *The Formation and Evolution of Planetary Systems*, ed. H. A. Weaver and L. Danly (Cambridge: Cambridge University Press), p. 1.
Winkler, K.-H., and Newman, M. J. 1980, *Ap. J.*, **236**, 201.
Yorke, H. W. 1979, *Astr. Ap.*, **80**, 308.
———. 1986, in *Astrophysical Radiation Hydrodynamics*, ed. K.-H. Winkler and M. L. Norman (Dordrecht: Reidel), p. 141.
———. 1988, in *Proc. 18th Advanced Course of the Swiss Society of Astrophysics and Astronomy, Radiation in Moving Gaseous Media*, ed. Y. Chmielewski, and T. Lanz (Sauverny-Versoix: Geneva Observatory), p. 193.
Yuan, C., and Cassen, P. 1985, *Icarus*, **64**, 435.

PETER BODENHEIMER: Lick Observatory, University of California, Santa Cruz, CA 95064

MICHAŁ RÓŻYCZKA: Warsaw University Observatory, Al. Ujazdowskie 4, PL-00478 Warszawa, Poland

JOEL TOHLINE: Department of Physics and Astronomy, Louisiana State University, Baton Rouge, LA 70803

HAROLD W. YORKE: Institut für Astronomie und Astrophysik, Universität Würzburg, am Hubland, D-8700 Würzburg, Federal Republic of Germany